catalysts

MDPI

Article

# Phosphotungstate-Based Ionic Silica Nanoparticles Network for Alkenes Epoxidation

**Xiaoting Li, Pingping Jiang *, Zhuangqing Wang and Yuandan Huang**

Received: 28 October 2015; Accepted: 14 December 2015; Published: 24 December 2015
Academic Editor: Michalis Konsolakis

The Key Laboratory of Food Colloids and Biotechnology, Ministry of Education,
School of Chemical and Material Engineering, Jiangnan University, Wuxi 214122, China;
advancedlxt@126.com (X.L.); 1050313227@vip.jiangnan.edu.cn (Z.W.); huangyuandan1989@163.com (Y.H.)
* Correspondence: ppjiang@jiangnan.edu.cn; Tel.: +86-135-0619-6132

**Abstract:** An inorganic-organic porous silica network catalyst was prepared by linking silica nanoparticles using ionic liquid and followed by anion-exchange with phosphotungstate. Characterization methods of FT-IR, TG, SEM, TEM, BET, *etc.*, were carried out to have a comprehensive insight into the catalyst. The catalyst was used for catalyzing cyclooctene epoxidation with high surface area, high catalytic activity, and convenient recovery. The conversion and selectivity of epoxy-cyclooctene could both reach over 99% at 70 °C for 8 h using hydrogen peroxide ($H_2O_2$) as an oxidant, and acetonitrile as a solvent when the catalyst was 10 wt. % of cyclooctene.

**Keywords:** silica nanoparticles; ionic liquid; network; phosphotungstate; catalyst; epoxidation

## 1. Introduction

Inorganic-organic hybrid [1–8] materials have attracted considerable interest as the combination of the features of different parts can generate high performance. As the development of nanoscale materials, $SiO_2$ has indeed stimulated remarkable scientific interest because of its excellent performance and promising applications in scientific and technological fields. In contrast to other inorganic materials, the preparation of $SiO_2$ nanoparticles has been very mature with a wide source of raw materials, and they possess the merits of high specific surfaces, as well as excellent thermal stabilities. Furthermore, the presence of a large number of silanol (Si–OH) groups on the surface makes it easily for surface organic functionalization [9,10]. Ionic liquids, a class of new type of green environmental protection organic compounds with outstanding properties, were introduced as the organic part, recently. The resulting materials can be applied into numerous fields, like catalysts, anion exchange, selective gas trapping, drug delivery, or electrochemistry [11].

The modification of silica nanoparticles with ionic liquids has been already reported by some researchers [12–14]. Ionic liquids are usually just grafted or absorbed onto the surface for next use. However, this is no longer a hot spot and novel method. Meanwhile, it remains separation problems if the nanoparticles are smaller than a certain size. For a few years now, the newly-arising challenge in the field of nanoparticle research is focusing on the development of specific materials based on assemblies of nanoparticles, which approaches to make use of the nanoparticle collective properties [15–20]. Thus, a silica network is being prepared by connecting silica nanoparticles with ionic liquid to take the advantage of covalent link of ionic liquid by two different parts.

Epoxides are important raw materials in chemical industrial production [21]. Polyoxometalates (POMs), as is known to all, have been widely used as epoxidation catalysts with $H_2O_2$ for their high efficient active centers [22–24]. However, POMs, themselves, are low efficient and soluble in some

epoxidation systems which results in the difficulty in separation of the catalysts. Therefore, ionic liquid-based POM hybrid catalysts come into being.

In this study, we first prepared a silica network by connecting silica nanoparticles with covalent-linked ionic liquid. This material was proved to be porous with high surface area. Phosphotungstic acid anions were then introduced into the material by ion exchange between Keggin-type $H_3PW_{12}O_{40}$ and ionic liquid as well as protonation of amino group. Ionic liquid had played an important role in two aspects: linking silica nanoparticles and introduction of an active center. The catalysts were used in catalytic epoxidation of olefin for the first time. Structural characteristics and catalytic performance of as-prepared catalysts were carried out to have a comprehensive insight into the catalyst. The study potentially propels the development of nanoparticle networks as promising materials for various fields to take advantage of the collective properties of nanoparticles.

## 2. Results and Discussion

### *2.1. Characterization*

#### 2.1.1. FT-IR Analysis

The basic modification moieties on the $SiO_2$ particles were characterized by FT-IR, which were shown in Figure 1. The bands at 3450 and 1630 $cm^{-1}$ were corresponding to stretching and bending vibrations of surface Si–OH groups on the surface of $SiO_2$. After grafting with silane coupling agent, the peak intensity decreased and new bands that assigned to the C–H stretching and bending rocking mode respectively appeared in the region of 2970 $cm^{-1}$ and 1460 $cm^{-1}$ (Figure 1b–e), which indicated the successful functionalization on the surface of $SiO_2$ particles. The other bands at 1100 $cm^{-1}$ and 814 $cm^{-1}$ were attributed to symmetric and anti-symmetric stretching vibration of Si–O–Si, and band at 960 $cm^{-1}$ was attributed to the Si–O stretching vibration of Si–OH. For PW (0.058)/$SiO_2$ $Im^+Cl^-$ $SiO_2$, a band at 890 $cm^{-1}$ appeared in Figure 1e, which was assigned to asymmetric stretching of W–$O_b$–W in the corner-shared octahedral of Keggin-type HPW. Other characteristic bands at 1080, 983, and 805 $cm^{-1}$ were all overlapped with the bands of $SiO_2$.

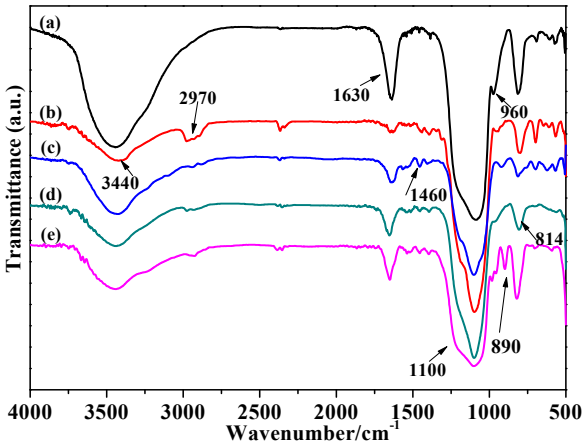


**Figure 1.** FT-IR spectra of (**a**) $SiO_2$; (**b**) $SiO_2$-Im; (**c**) $SiO_2$-Cl; (**d**) $SiO_2$ $Im^+Cl^-$ $SiO_2$; (**e**) PW(0.058)/$SiO_2$ $Im^+Cl^-$ $SiO_2$.

#### 2.1.2. Thermal Stability and Structure

The TG analyses of $SiO_2$, $SiO_2$-Cl, $SiO_2$-Im, $SiO_2$ $Im^+Cl^-$ $SiO_2$, and PW (0.058)/$SiO_2$ $Im^+Cl^-$ $SiO_2$ were shown in Figure 2. For the pure $SiO_2$ nanoprticles (Figure 2a), the weight loss of 5.65 wt. % could be only observed before 100 °C, which was assigned to the desorption of water. No weight loss could be seen even with the increasing of temperature to 800 °C. In reality, the formed ionic units

of imidazolium presents a higher thermal stability than the aromatic precursors. The precursors started to decompose before 200 °C, while the imidazolium mainly decomposes around 300 °C. From Figure 2b,c, $SiO_2$-Cl started to decompose at 180 °C, $SiO_2$-Im started to decompose at 120 °C, and the main weight loss was around 400 °C. From Figure 2d, the first stage ranging from 25 to 120 °C was ascribed to the elimination of adsorbed water. After 120 °C the unreacted organic groups started to decompose and the weight loss around 300 °C was mainly attributed to the decomposition of imidazolium ionic units, which could verify the occurrence of nucleophilic reactions, on one hand. For the PW(0.058)/$SiO_2$ $Im^+Cl^-$ $SiO_2$ (Figure 2e), the mass loss after 300 °C also contained the collapse of PW anions in the remainder form of $P_2O_5$ and $WO_3$.

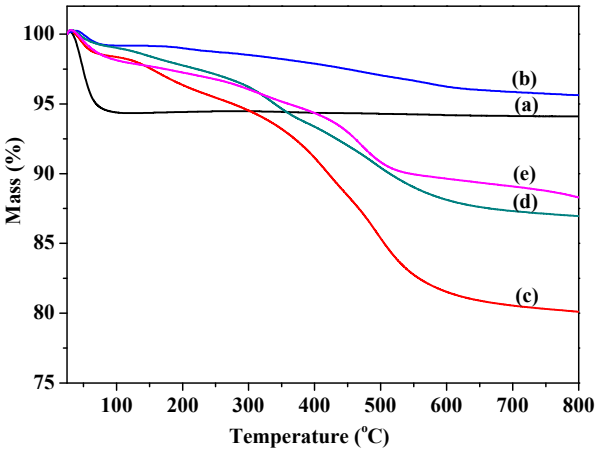


**Figure 2.** Thermogravimetric curves of (**a**) $SiO_2$; (**b**) $SiO_2$-Cl; (**c**) $SiO_2$-Im; (**d**) $SiO_2$ $Im^+Cl^-$ $SiO_2$; and (**e**) PW(0.058)/$SiO_2$ $Im^+Cl^-$ $SiO_2$.

### 2.1.3. SEM, EDS, TEM, and DLS Characterization

The morphology changes between $SiO_2$ nanoparticles and the modified product of $SiO_2$-Cl, $SiO_2$-Im, and $SiO_2$ $Im^+Cl^-$ $SiO_2$ were provided by the SEM and TEM images presented in Figure 3. Figure 3a,b were the SEM images for $SiO_2$ nanoparticles before reaction, which presented scattered and small particles size of $SiO_2$. The particle size could be observed in TEM in Figure 3f,g with an average of 15 nm diameter which was in slight agglomeration. After functionalization, the particle morphology of $SiO_2$-Cl and $SiO_2$-Im had almost no change (showed in (c) and (d)) compared to $SiO_2$ nanoparticles. Figure 3e,h showed the SEM and TEM micrographs after linking nanoparticles through the ionic liquid-like bond. The product, by observation of "islands", connected into a larger group, like sponge-cake with dispersed holes.

In order to get a profound insight into the microscopic structure, scanning SEM-energy dispersive spectroscopy (EDS) elemental mapping images of catalyst PW(0.058)/$SiO_2$-Im-$SiO_2$ was produced, and the results were shown in Figure 3i. Si, O, N, Cl, P, and W were uniformly distributed in this catalyst.

DLS (Dynamic Light Scattering) was carried out after dispersing the samples in ethanol with previous sonication and the results were shown in Figure 4. It also indicated that the particle size of the product $SiO_2$ $Im^+Cl^-$ $SiO_2$ was much larger than the one before reaction, which corresponded to the SEM and TEM micrographs. For Figure 4A, a diffraction peak could be observed around 30 nm. The result was larger than the measurement by TEM micrographs, which was due to the slight agglomeration. When reacting with *N*-(3-triethoxysilylpropyl)-4,5-dihydroimidazol, the particle size was slightly increased in Figure 4B. Nevertheless, for the resulted $SiO_2$ $Im^+Cl^-$ $SiO_2$, the most average size showed in Figure 4C was at 700 nm after nucleophilic reaction. The smaller size distribution was due to the incomplete or partial reaction of the functionalized silica particles. Overall, this size was much larger than $SiO_2$, also indicating the change after the reaction.

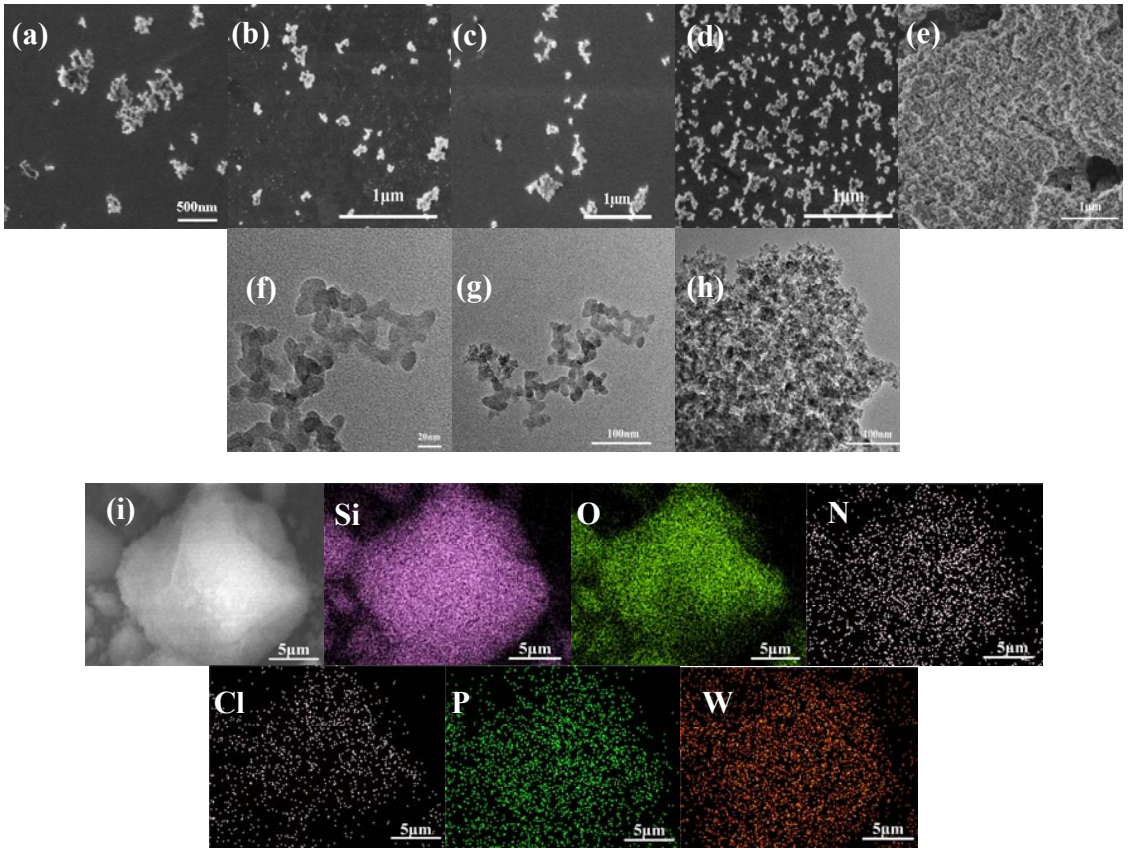


**Figure 3.** SEM, TEM and EDS images at different magnifications. (**a**,**b**) for SEM of $SiO_2$; (**c**) for SEM of $SiO_2$-Cl; (**d**) for SEM of $SiO_2$-Im; (**e**) for SEM of $SiO_2$ $Im^+Cl^-$ $SiO_2$; (**f**,**g**) for TEM of $SiO_2$; and (**h**) for TEM of $SiO_2$ $Im^+Cl^-$ $SiO_2$ respectively; (**i**) for EDS elemental mapping images of the Si, O, N, Cl, P, and W, respectively.

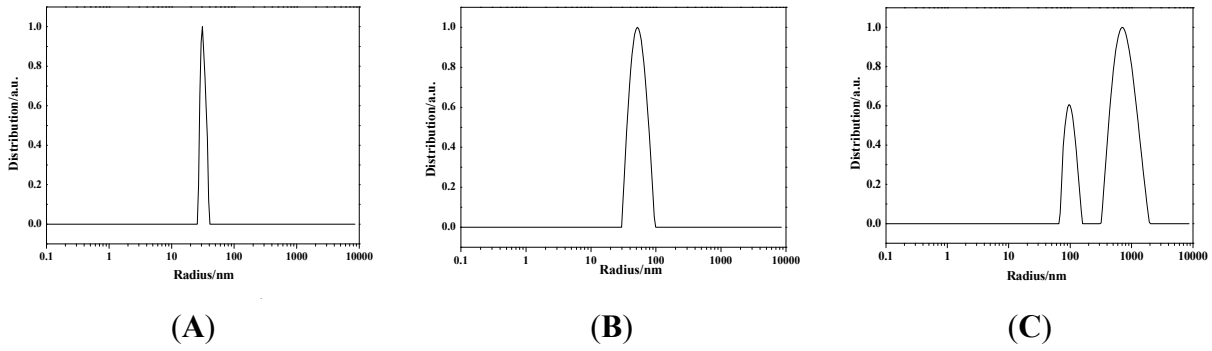


**Figure 4.** DLS measurement of (**A**) the starting $SiO_2$ nanoparticles; (**B**) $SiO_2$-Im; and (**C**) resultant $SiO_2$ $Im^+Cl^-$ $SiO_2$.

### 2.1.4. Nitrogen Sorption

The porous characteristic of the materials were investigated by Brunauer-Emmet-Teller (BET) method. The $N_2$ adsorption-desorption isotherms and corresponding pore size distribution curves were shown in Figure 5 (the curves of $PW/SiO_2$ $Im^+Cl^-$ $SiO_2$ were particularly similar, so $PW(0.058)/SiO_2$ $Im^+Cl^-$ $SiO_2$ was chose as representative). All samples displayed typical type-IV isotherms with a clear adsorption-desorption hysteresis loops at the relative pressure of $0.8 < P/P_0 < 1$ (Figure 5, left) as well as broad pore size distribution (Figure 5, right). For the $SiO_2$ nanoparticles, the pore size was mainly distributed in less than 2 nm, which was due to the micropores of nanoparticles

themselves. The size formed above 2 nm was mainly due to the accumulation between the particles. However, when linked by ionic liquid, the $SiO_2$ network and its catalyst showed more regular in pore size distribution between 20–40 nm. Data of surface area, pore diameter, and pore volume were presented in Table 1. The BET specific surface area of the prepared $SiO_2$ particles (entry 1) was as high as 381 $m^2 \cdot g^{-1}$ and the average pore size was 11.2 nm. When modified by organic reagents and then linked by nucleophilic reaction, specific surface of $SiO_2$ network (entry 2) was obviously lower than the pure $SiO_2$ due to the introduction of the organic moieties. After introducing phosphotungstic acid anions into the material by ion exchange, the specific surface of PW($x$)/$SiO_2$ $Im^+Cl^-$ $SiO_2$ (entries 3–6) also decreased and were lower than the $SiO_2$ network. Meanwhile, compared to the pure $SiO_2$, the $SiO_2$ network and its catalysts exhibited an increase of pore size and pore volume. In particular, the pore size seemed more centralized. This increased the contact area of the substrate and catalysts and led to better catalytic effect. Meanwhile, increased PW anions loading of PW($x$)/$SiO_2$ $Im^+Cl^-$ $SiO_2$ led to a gradual decrease in pore volume and average pore size (entries 3–6).

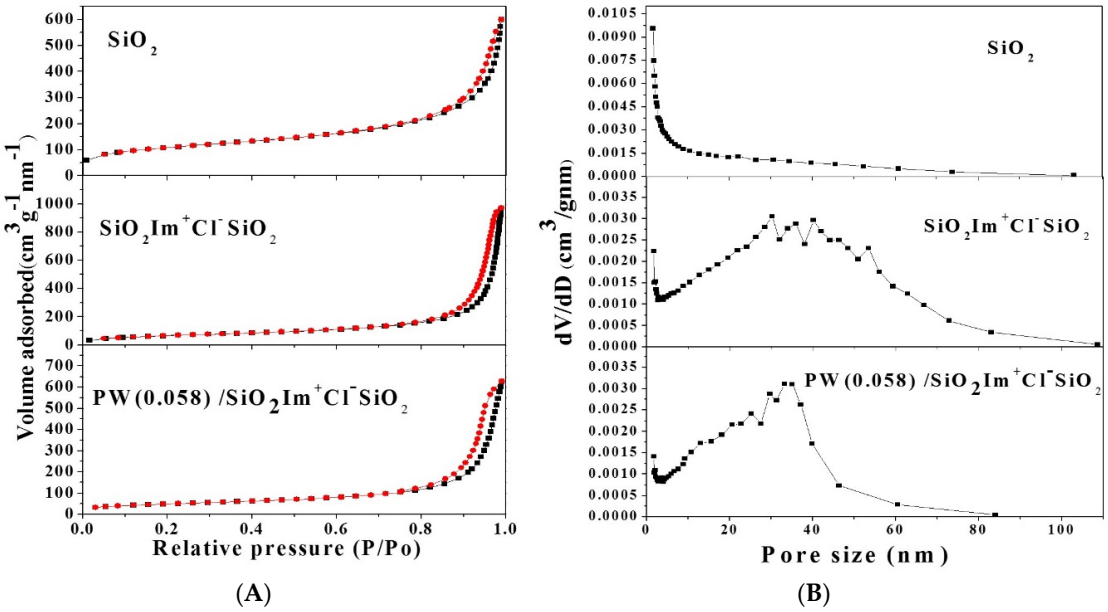


**Figure 5.** Nitrogen adsorption-desorption isotherms (**A**) and pore size distribution (**B**) of the samples $SiO_2$, $SiO_2$ $Im^+Cl^-$ $SiO_2$, and PW/$SiO_2$ $Im^+Cl^-$ $SiO_2$.

**Table 1.** BET parameters of the $SiO_2$, $SiO_2$ $Im^+Cl^-$ $SiO_2$, and PW($x$)/$SiO_2$ $Im^+Cl^-$ $SiO_2$.

| Entry | Compound | SBET ($m^2 \cdot g^{-1}$) | Vp ($cm^3 \cdot g^{-1}$) | Average Pore Size (nm) |
|---|---|---|---|---|
| 1 | $SiO_2$ | 381 | 0.93 | 11.2 |
| 2 | $SiO_2$ $Im^+Cl^-$ $SiO_2$ | 242 | 1.50 | 24.1 |
| 3 | PW(0.035)/$SiO_2Im^+Cl^-SiO_2$ | 182 | 1.24 | 24.0 |
| 4 | PW(0.058)/$SiO_2Im^+Cl^-SiO_2$ | 176 | 1.07 | 24.0 |
| 5 | PW(0.074)/$SiO_2Im^+Cl^-SiO_2$ | 168 | 1.01 | 22.4 |
| 6 | PW(0.17)/$SiO_2Im^+Cl^-SiO_2$ | 159 | 0.93 | 20.3 |

### 2.1.5. More Evidence of the Synthesis of the Network

In order to further confirm the occurrence of nucleophilic substitution between the imidazoline functional group and chloroalkyl group, anion exchange experiment was carried out as an indirect proof. Once the nucleophilic substitution happened, the chloride ion was easily exchanged by the fluorinated anion to obtain the $SiO_2$ $Im^+BF_4^-$ $SiO_2$ and NaCl. First, we detected chloride ions in the solvent and washing phase by the signature of the halide salts in the X-ray diffraction pattern after

drying (Figure 6). In the XRD pattern, the obtained salt reflection was marked with a star and was consistent with NaCl. The other Bragg peaks belonged to the fluorinated salt which was in an excess in order to confirm the exchange. Next, EDX analysis of the hybrid material $SiO_2$ $Im^+BF_4^-$ $SiO_2$, obtained after the exchange reaction also showed the existence of newly-introduced anions (Figure 7). Typical peaks of fluorine from the newly exchanged anions could be obviously observed while the boron was hidden by the carbon peak. After the exchange reaction, it was noted that chlorine could still be observed in a small amount. The presence of chlorine was due to the residue alkyl chloride groups which did not react with APTES or the residue chlorine ions which were not exchanged.

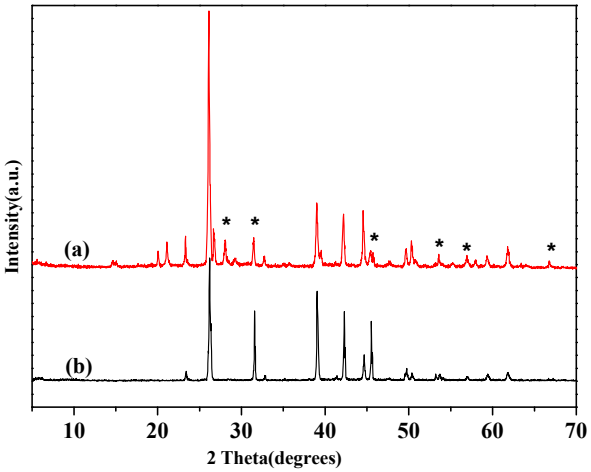


**Figure 6.** XRD analyses of (**a**) the exchange solvent, after separation and washing; (**b**) $NaBF_4$. The obtained salt reflection was marked with a star and was consistent with NaCl.

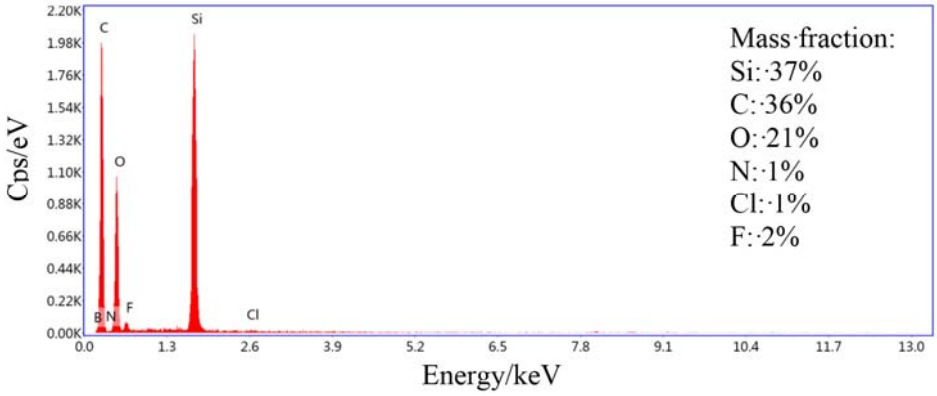


**Figure 7.** EDX spectra of the resulting materials.

## 2.2. Catalytic Performances

It is known to all that the Keggin-type $[PW_{12}O_{40}]^{3-}$ (PW) can be degraded to peroxo-active species, $[PW_4O_8(O_2)_8]^{3-}$ species, by excess hydrogen peroxide, which is the active species in alkenes epoxidations [25]. The solvent has a great influence on the activity of catalytic reaction and acetonitrile is commonly used in epoxidation reaction as an efficient solvent. Moreover, using $H_2O_2$ as an oxygen source can do great benefits on the environment and industry [26]. Thus, Table 2 listed the catalytic performance of different catalysts for the epoxidation of cyclooctene in acetonitrile using aqueous 30% $H_2O_2$ as an oxidant. The results showed that the catalyst $PW/SiO_2$ $Im^+Cl^-$ $SiO_2$ had much better catalytic effect than the Keggin-type $H_3PW_{12}O_{40}$. One reason was the super-hydrophobic of $H_3PW_{12}O_{40}$, which made it difficult to contact with the oily substrates. Meanwhile, the cations of imidazolium and $NH_2^+$ in imidazoline made it easier for the redox of PW. Physical loading of HPW

on the pure $SiO_2$ nanoparticles was carried out and the catalytic activity was very low, which also illustrated the serviceability of $SiO_2$ $Im^+Cl^-$ $SiO_2$ for loading the PW anions. In order to further compare the catalytic activity of the network catalysts with traditional silica grafted ionic liquid catalyst, we also performed a catalytic reaction in the presence of the imidazolium and the silica particles labeled as HPW/$SiO_2$-IL which was prepared by nucleophilic reaction between $SiO_2$-Cl and methylimidazole, and then reacted with phosphotungstic acid. The catalytic activity showed that the conversion was lower than the network catalysts with similar selectivity (Table 2, entry 4), which demonstrated that the formed network catalysts could lead to high conversion and selectivity.

**Table 2.** Catalytic performances of cyclooctene with various catalysts.

| Catalysts | Conversion (%) | | | | Selectivity (%) | | | |
|---|---|---|---|---|---|---|---|---|
| | 2 h | 4 h | 6 h | 8 h | 2 h | 4 h | 6 h | 8 h |
| $SiO_2$ | - | - | - | - | - | - | - | - |
| HPW | 4.9 | 8.6 | 11.2 | 14.2 | 70.3 | 67.9 | 61.8 | 43.2 |
| HPW/$SiO_2$ | 0.8 | 1.6 | 4.4 | 6.6 | 36.8 | 34.5 | 35.8 | 32.4 |
| HPW/$SiO_2$-IL | 30.5 | 52.7 | 72.4 | 79.8 | 98.7 | 98.1 | 97.4 | 97.0 |
| PW(0.035)/$SiO_2Im^+Cl^-SiO_2$ | 54.3 | 68.4 | 76.5 | 84.1 | 98.5 | 98.2 | 97.9 | 96.9 |
| PW(0.058)/$SiO_2Im^+Cl^-SiO_2$ | 77.2 | 88.8 | 94.4 | 99.4 | 99.4 | 99.4 | 99.3 | 99.2 |
| PW(0.074)/$SiO_2Im^+Cl^-SiO_2$ | 68.5 | 78.2 | 91.1 | 93.5 | 99.3 | 98.4 | 98.9 | 98.9 |
| PW(0.17)/$SiO_2Im^+Cl^-SiO_2$ | 45.3 | 63.6 | 70.2 | 77.6 | 98.7 | 98.1 | 98.7 | 98.2 |

Reaction conditions: cyclooctene: 2 mmol, acetonitrile: 5 mL, $H_2O_2$: 6 mmol, catalysts: 0.02 g, temperature 70 °C.

Furthermore, Table 2 also showed that the loading of PW anions of PW/$SiO_2Im^+Cl^-SiO_2$ affected the catalytic activity of the catalysts. This was correlation with the amount of active sites in the catalyst and the inside structure of material. Obviously, PW(0.058)/$SiO_2Im^+Cl^-SiO_2$ showed the best activity. When the loading of PW anions was less than 0.058, the conversion decreased accordingly. However, excessive PW loading resulted in the agglomeration of excessive HPW in the channel, which might change the specific surface area and pore volume, therefore, led to the decrease of catalytic activity.

To investigate the importance of the IL moiety, the imidazoline based PW/$SiO_2$-Im was prepared by stirring 0.6 g HPW with 1 g $SiO_2$-Im, and the loading of PW were *ca.* 0.082 mmol/g. The catalytic activity and reusability were compared in Table 3. Imidazoline-modified $SiO_2$ can be protonated with HPW. The results showed that the catalyst of PW/$SiO_2$-Im offered even higher conversion than PW(0.058)/$SiO_2Im^+Cl^-SiO_2$ in the first run. This is because of the increased protonating of $SiO_2$-Im per unit mass leading to more PW loading, and the PW(0.058)/$SiO_2Im^+Cl^-SiO_2$ also contains the part of $SiO_2$-Cl. However, the reusability of PW/$SiO_2$-Im was far less active than the catalyst of PW(0.058)/$SiO_2$ $Im^+Cl^-SiO_2$. There were two possible reasons: one was that the stability of $NH_2^+$ in imidazoline was low and the other was that the recovery efficiency of individual $SiO_2$ nanoparticles was much lower than the collective $SiO_2$ network on account of the catalysts size.

**Table 3.** Catalytic reusability of PW(0.058)/$SiO_2Im^+Cl^-SiO_2$ and PW(0.082)/$SiO_2$-Im for the epoxidation of cyclooctene.

| Run [a] | PW(0.058)/$SiO_2Im^+Cl^-SiO_2$ | | PW(0.082)/$SiO_2$-Im | |
|---|---|---|---|---|
| | Conversion (%) | Selectivity (%) | Conversion (%) | Selectivity (%) |
| 1 | 94.4 | 99.3 | 96.0 | 98.2 |
| 2 | 88.7 | 97.5 | 27.1 | 87.3 |
| 3 | 82.1 | 95.1 | 25.8 | 81.6 |
| 4 | 75.2 | 94.6 | 18.6 | 78.3 |

The reusability experiment was carried out by adding the residual catalyst in the next reaction after centrifugation and drying without any change of other components. [a] Reaction conditions: cyclooctene: 2 mmol, acetonitrile: 5 mL, $H_2O_2$: 6 mmol, catalysts: 0.02 g, temperature: 70 °C, reaction time: 6 h.

### 2.2.1. Effects of Temperature and Time

Each chemical reaction was accompanied by thermal effects. The same reaction carried out at different temperatures would result in quite different results. The reaction time was an important basis to judge it effective or not. The effects of temperature and time on the epoxidation of cyclooctene using catalyst PW(0.058)/$SiO_2$Im$^+$Cl$^-$$SiO_2$ were shown in Figure 8. It was observed that with the increase of temperature, the molecular energy, and relative content of activated molecules increased, which increased the effective collision between the reactant molecules, thereby improving the conversion. However, the increase of temperature also increased the possibility of ring rupture, resulting in the decrease of selectivity. When temperature reached 70 °C, the reaction had tended to balance. However, the conversion decreased at 80 °C and the selectivity was in a sharp decline which might be due to the excessive activation of the catalyst. And with the increase of reaction time, the conversion increased while selectivity decreasing. As a whole, the conversion and selectivity were both higher than 90% at 70 °C in 6 h; specifically, 94.4% and 99.3%, respectively.

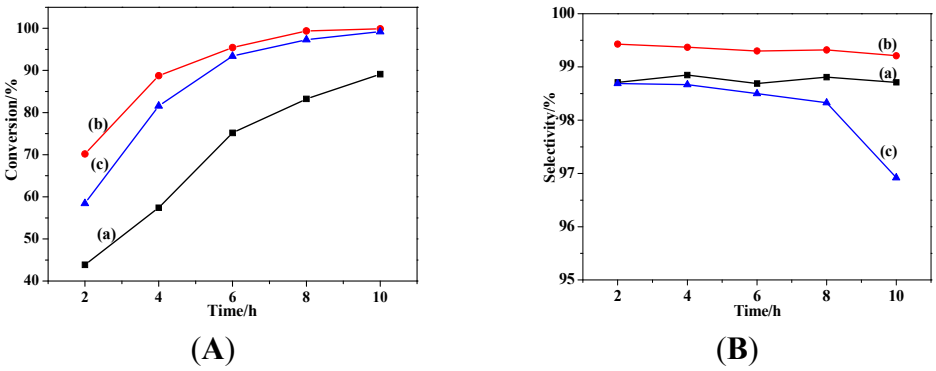


**Figure 8.** Effect of temperature and time on (**A**) conversion; and (**B**) selectivity. (a): 60 °C; (b): 70 °C; and (c): 80 °C.

### 2.2.2. Effect of Catalyst Dosage

The influences of different catalyst amounts were investigated and the results were shown in Figure 9. It was indicated that the conversion increased with the increase of catalyst amount, but further improved slightly when the amount was over 300 mg. The selectivity had almost no change when the amount was over 200 mg. Taking economics and green chemistry into consideration, a low catalyst amount (200 mg) was used in further experiments.

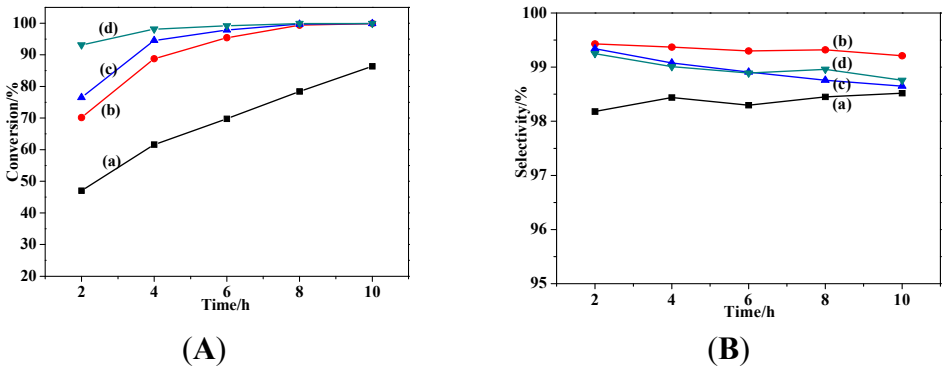


**Figure 9.** Effect of temperature and time on (**A**) conversion and (**B**) selectivity. (a): 0.01 g; (b):0.02 g; (c): 0.03 g; (d): 0.04 g.

#### 2.2.3. Effect of Solvent

In order to investigate the general application of the synthetic catalyst in different solvents, the influences of solvents on the oxidation of cyclooctene were studied and the results were summarized in Table 4. Acetonitrile, methanol, ethanol, chloroform, 1,2-dichloroethane, and ethyl acetate were used as solvents. The results demonstrated that the solvents were general relevant to alkenes epoxidation, especially for acetonitrile, methanol, and chloroform. In particular, the catalytic reaction was more suitable in the polar solvent. Due to the high boiling point and stable selectivity of the product, acetonitrile was, thus, chosen as the reaction medium in our experiment.

**Table 4.** Effect of solvents on epoxidation of cyclooctene.

| Entry | Solvent | Boiling Point (°C) | Conversion | | Selectivity | |
|---|---|---|---|---|---|---|
| | | | 4 h | 8 h | 4 h | 8 h |
| 1 | Acetonitrile | 81.6 | 88.8 | 99.4 | 99.4 | 99.2 |
| 2 | Methanol | 64.5 | 92.9 | 96.8 | 99.1 | 96.6 |
| 3 | Ethanol | 78.2 | 52.0 | 77.1 | 98.8 | 98.8 |
| 4 | Chloroform | 61.2 | 98.9 | 100.0 | 98.6 | 96.6 |
| 5 | 1,2-Dichloroethane | 83.5 | 8.8 | 15.0 | 94.0 | 93.6 |
| 6 | Ethyl acetate | 78.3 | 4.5 | 5.5 | 85.8 | 88.2 |

Reaction conditions: cyclooctene: 2 mmol, solvent: 5 mL, $H_2O_2$: 6 mmol, catalysts: 0.02 g, temperature: 70 °C.

## 3. Experimental Section

### *3.1. Materials and Methods*

*N*-(3-triethoxysilylpropyl)-4,5-dihydroimidazol and 3-aminopropyl-trimethoxysilane (APTES) were purchased from Meryer (Meryer, Shanghai, China). Other commercially-available chemicals were bought from local suppliers (Sinopharm Chemical Reagent, Beijing, China). All reagents were purified by standard procedures before use. FT-IR spectra were obtained as potassium bromide pellets in a Nicolet 360 FT-IR thermoscientific spectrometer in the 4000–400 $cm^{-1}$ region (Thermo Fisher Scientific, Waltham, MA, USA). The elemental analyses were performed on a CHN elemental analyzer (Elementar, Hanau, HE, Germany). TG analysis was carried out with a STA409 instrument in dry air at a heating rate of 10 °C· $min^{-1}$ (Mettler Toledo, Zurich, Switzerland). SEM image was performed on a HITACHI S-4800 field-emission scanning electron microscope (Hitachi, Tokyo, Japan). Transmission electron microscopic (TEM) photographs of the prepared samples were taken in JEOL JEM 2100 electron microscope under an accelerating voltage of 200 kV (JEOL, Tokyo, Japan). The metal loading of the host materials of Tungsten were determined by inductively-coupled plasma atomic emission spectroscopy (ICP-AES) on a Perkin-Elmer AA-300 spectrophotometer (Shimadzu, Kyoto, Japan). Nitrogen adsorption/desorption isotherms were measured at −196 °C using a Quantachrome Quadrasorb SI automated gas sorption system (Micromeritics instrument corp, Atlanta, GA, USA). Samples were degassed under vacuum for 5 h at 120 °C. The micropore volume was obtained with the *t*-plot method, while the Brunauer-Emmet-Teller (BET) method was applied to calculate the specific surface area. Pore size distributions were evaluated from desorption branches of nitrogen isotherms using the BJH model. The total pore volume was determined at $P/P_0$ 0.95. The X-ray diffraction (XRD) pattern of the material was recorded on a Bruker D8 advanced powder X-ray diffractometer using Cu Ka (k = 1.5406 Å) as the radiation source in 2θ range of 4°–70° with a step size of 4° and a step time of 1 s (Bruker Axs Gmbh, Karlsruhe, BW, Germany). DLS experiments were carried out with previous sonication of the samples. The run time of the measurements was 10 s. Every size distribution curve was obtained by averaging six measurements. The apparatus was an ALV/DLS/SLS-5022F light scattering electronic spectrometer (ALV-GmbH, Langen, Germany).

### 3.2. Catalyst Preparation

Silica nanoparticles, as well as the surface functionalization of the silica nanoparticles with *N*-(3-triethoxysilylpropyl)-4,5-dihydroimidazol and APTES, were prepared according to literature with minor modification [27]. The typical preparation procedure of the catalyst was in Scheme 1.

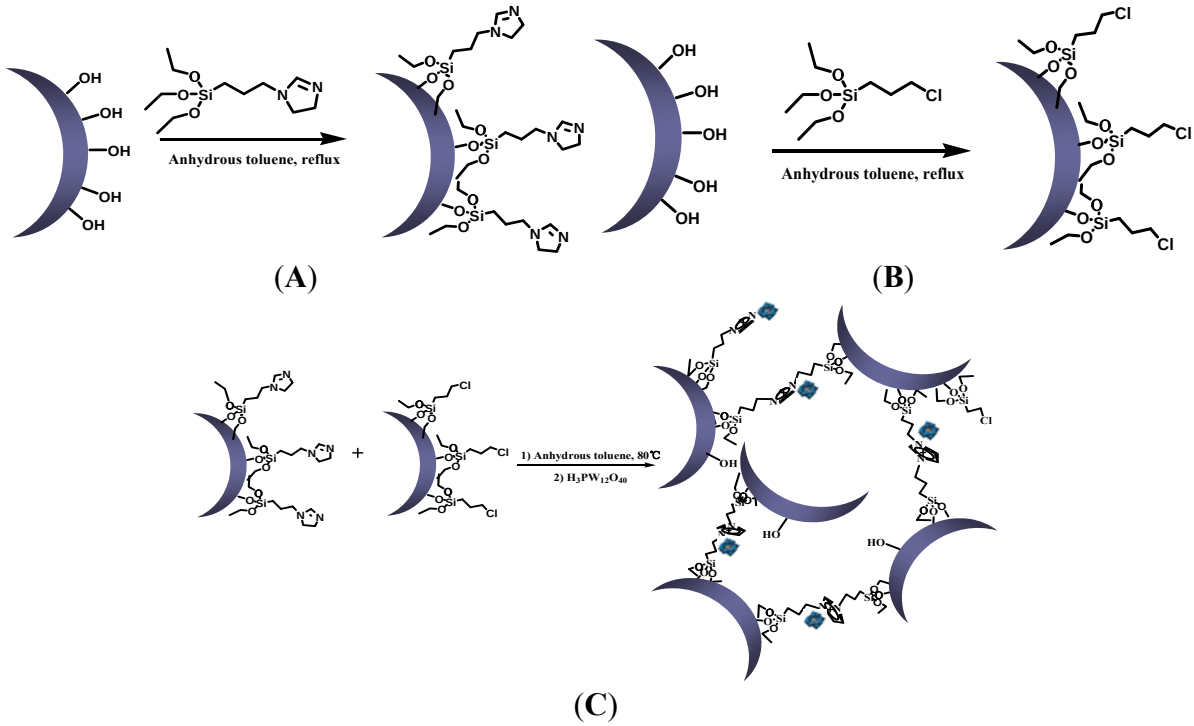


**Scheme 1.** Typical preparation procedure of the catalysts PW(*x*)/$SiO_2$ $Im^+Cl^-$ $SiO_2$. (**A**) Synthesis of $SiO_2$-Im; (**B**) Synthesis of $SiO_2$-Cl; (**C**) Synthesis of PW(*x*)/$SiO_2$ $Im^+Cl^-$ $SiO_2$.

#### 3.2.1. Synthesis of Silica Nanoparticles

74 μL ammonia solution (25%–28%) and 1.98 g (110 mmol) water were added to 100 mL absolute methanol in a 250 mL round bottom flask. The solution was stirred for 5 min before adding dropwise 10.41 g (500 mmol) TEOS. The final solution was stirred for three days at ambient temperature. The resulting solid was centrifuged and washed with methanol and water several times, and dried under vacuum.

#### 3.2.2. Synthesis of Modified Silica Nanoparticles

0.6 g (0.01 mol) previously prepared silica nanoparticle was dispersed in 50 mL anhydrous toluene by sonication for 60 min. Then 0.005 mol *N*-(3-triethoxysilylpropyl)-4,5-dihydroimidazol (or APTES) was added dropwise. The solution was stirred under 110 °C for 24 h. The product was filtered, washed in a Soxhlet apparatus with diethyl ether and dichloromethane for 24 h, and then dried at 50 °C under vacuum. The obtained powder was named as $SiO_2$-Im and $SiO_2$-Cl, respectively.

#### 3.2.3. Synthesis of Silica Nanoparticle Network

The synthesis was driven by a nucleophilic substitution occurring between an imidazoline functional group and a chloroalkyl group present on the surface of the silica nanoparticles. 0.5 g silica nanoparticles modified with *N*-(3-triethoxysilylpropyl)-4,5-dihydroimidazol and 0.5 g silica nanoparticles modified with APTES were introduced into a 100 mL round bottom flask with 50 mL anhydrous toluene. The solution was stirred over 2 days at 70 °C and filtered, washed,

finally dried under vacuum. A pale yellow powder was obtained and labelled as $SiO_2$ $Im^+Cl^-$ $SiO_2$. Elemental analysis: found C: 7.25 wt. %, H: 1.45 wt. %, N: 1.96 wt. %.

#### 3.2.4. Synthesis of Phosphotungstate-Loaded Silica Nanoparticle Network

Catalysts of PW($x$)/$SiO_2$ $Im^+Cl^-$ $SiO_2$ with different $H_3PW_{12}O_{40}$ loadings on $SiO_2$ $Im^+Cl^-$ $SiO_2$ were prepared by following strategy. 1.0 g silica nanoparticle network was dispersed in 20 mL deionized water and then added dropwise into an aqueous solution (20 mL) with various amount of $H_3PW_{12}O_{40}$ (0.2 g, 0.6 g, 1.0 g, 1.4 g). The solution was stirred for 24 h at ambient temperature. Upon centrifugation, the precipitate was washed with deionized water several times, and then dried in vacuum overnight at room temperature. The obtained catalysts were labelled as PW($x$)/$SiO_2$ $Im^+Cl^-$ $SiO_2$, where $x$ was the loading amount of PW. The PW loading could be calculated by ICP-AES. The results showed that the loading of PW were *ca.* 0.035, 0.058, 0.074, or 0.17 mmol/g, respectively.

#### 3.2.5. Anion Exchange Experiment

The starting compound $SiO_2$ $Im^+Cl^-$ $SiO_2$ was dispersed in 25 mL acetone. The salt $NaBF_4$ for the exchange was added in mass in a ratio of 1:1, compared to the starting compound. The dispersion was stirred for 24 h at room temperature. Then, the resultant product $SiO_2$ $Im^+BF_4^-$ $SiO_2$ was centrifuged and washed with acetone and deionized water. The solvent and washing phases were combined and evaporated under vacuum. The salt obtained after evaporation and was dried in vacuum over $P_2O_5$. White powders are obtained as $NaBF_4$ and NaCl.

### *3.3. Catalytic Performance*

Cyclooctene (2 mmol), $CH_3CN$ (5 mL), and catalyst (0.02 g) were added to a 25 mL flask. The reaction started after the addition of aqueous $H_2O_2$ (30 wt. %, 6 mmol) at a definite temperature within 10 min under vigorous stirring. After reaction, the product mixture was analyzed by gas chromatography mass spectrometry (GC-MS). The catalyst was recovered by centrifugation, dried and used for the next run.

## 4. Conclusions

In this research, a silica network catalyst was prepared by connecting silica nanoparticles with ionic liquid and followed reacting with phosphotungstate. A series of characterization methods were carried out to confirm the successful synthesis of the material. The synthetic catalyst was effective heterogeneous catalyst for the epoxidation of cyclooctene with $H_2O_2$. Conversion and selectivity of epoxy-cyclooctene could both reach over 99% at 70 °C for 8 h using hydrogen peroxide as an oxidant in acetonitrile. Compared with silica nanoparticles, the reported work demonstrated that the inorganic-organic hybrid silica network performed as a more promising material in various fields for its collective properties: better pore structure, much easier to separate and, thus, to recycle.

**Acknowledgments:** Thanks for the Cooperative Innovation Foundation of Industry, Academy and Research Institutes (BY2013015-10) in Jiangsu Province of China and the Fundamental Research Funds for the Central Universities (JUSRP51507).

**Author Contributions:** The experimental work and drafting of the manuscript were mainly done by X.L., assisted by Z.W., who carried out some catalyst characterization. Y.H. contributed the materials and assisted the analyses of some experiment results. P.J. conceived and designed the experiment. All authors have approved for the final version of the manuscript.

**Conflicts of Interest:** The authors declare no conflict of interest.

## References


1. Zhu, C.; Guo, S.; Zhai, Y.; Dong, S. Layer-by-Layer Self-Assembly for Constructing a Graphene/Platinum Nanoparticle Three-Dimensional Hybrid Nanostructure Using Ionic Liquid as a Linker. *Langmuir* **2010**, *26*, 7614–7618. [CrossRef] [PubMed]
2. Corma, A.; Iborra, S.; Llabres i Xamena, F.X.; Monton, R.; Calvino, J.J.; Prestipino, C. Nanoparticles of Pd on Hybrid Polyoxometalate-Ionic Liquid Material: Synthesis, Characterization, and Catalytic Activity for Heck Reaction. *J. Phys. Chem. C* **2010**, *114*, 8828–8836. [CrossRef]
3. Zhang, Q.; Zhang, L.; Zhang, J.Z.; Li, J. Preparation of 1-Propyl-3-Methyl-Imidazolium Chloride Functionalized Organoclay for Protein Immobilization. *Sci. Adv. Mater.* **2009**, *1*, 55–62. [CrossRef]
4. Karousis, N.; Economopoulos, S.P.; Sarantopoulou, E.; Tagmatarchis, N. Porphyrin counter anion in imidazolium-modified graphene-oxide. *Carbon* **2010**, *48*, 854–860. [CrossRef]
5. Vangeli, O.C.; Romanos, G.E.; Beltsios, K.G.; Fokas, D.; Kouvelos, E.P.; Stefanopoulos, K.L.; Kanellopoulos, N.K. Grafting of Imidazolium Based Ionic Liquid on the Pore Surface of Nanoporous Materials-Study of Physicochemical and Thermodynamic Properties. *J. Phys. Chem. B* **2010**, *114*, 6480–6491. [CrossRef] [PubMed]
6. Trilla, M.; Pleixats, R.; Man, M.W.C.; Bied, C. Organic-inorganic hybrid silica materials containing imidazolium and dihydroimidazolium salts as recyclable organocatalysts for Knoevenagel condensations. *Green. Chem.* **2009**, *11*, 1815–1820. [CrossRef]
7. Tonle, I.K.; Letaief, S.; Ngameni, E.; Detellier, C. Nanohybrid materials from the grafting of imidazolium cations on the interlayer surfaces of kaolinite. Application as electrode modifier. *J. Mater. Chem.* **2009**, *19*, 5996–6003. [CrossRef]
8. Crees, R.S.; Cole, M.L.; Hanton, L.R.; Sumby, C.J. Synthesis of a Zinc(II) Imidazolium Dicarboxylate Ligand Metal-Organic Framework (MOF): A Potential Precursor to MOF-Tethered *N*-Heterocyclic Carbene Compounds. *Inorg. Chem.* **2010**, *49*, 1712–1719. [CrossRef] [PubMed]
9. Yuan, D.; Liu, Z.L.; Tay, S.W.; Fan, X.S.; Zhang, X.W.; He, C.B. An amphiphilic-like fluoroalkyl modified $SiO_2$ nanoparticle@Nafion proton exchange membrane with excellent fuel cell performance. *Chem. Commun.* **2013**, *49*, 9639–9641. [CrossRef] [PubMed]
10. Zhang, J.; Jiang, P.P.; Shen, Y.R.; Zhang, W.J.; Li, X.T. Molybdenum(VI) complex with a tridentate Schiff base ligand immobilized on SBA-15 as effective catalysts in epoxidation of alkenes. *Micropor. Mesopor. Mat.* **2015**, *206*, 161–169. [CrossRef]
11. Czakler, M.; Litschauer, M.; Fottinger, K.; Peterlik, H.; Neouze, M.A. Photoluminescence as Complementary Evidence for Short-Range Order in Ionic Silica Nanoparticle Networks. *J. Phys. Chem. C* **2010**, *114*, 21342–21347. [CrossRef] [PubMed]
12. Yamaguchi, K.; Yoshida, C.; Uchida, S.; Mizuno, N. Peroxotungstate Immobilized on Ionic Liquid-modified Silica as a Heterogeneous Epoxidation Catalyst with Hydrogen Peroxide. *J. Am. Chem. Soc.* **2005**, *127*, 530–531. [CrossRef] [PubMed]
13. Han, L.; Shu, Y.; Wang, X.F.; Chen, X.W.; Wang, J.H. Encapsulation of silica nano-spheres with polymerized ionic liquid for selective isolation of acidic proteins. *Anal. Bioanal. Chem.* **2013**, *405*, 8799–8806. [CrossRef] [PubMed]
14. Bagheri, M.; Masteri-Farahani, M.; Ghorbani, M. Synthesis and characterization of heteropolytungstate-ionic liquid supported on the surface of silica coated magnetite nanoparticles. *J. Magn. Magn. Mater.* **2013**, *327*, 58–63. [CrossRef]
15. Roeser, J.; Kronstein, M.; Litschauer, M.; Thomas, A.; Neouze, M.A. Ionic Nanoparticle Networks as Solid State Catalysts. *Eur. J. Inorg. Chem.* **2012**, *32*, 5305–5311. [CrossRef]
16. Neouze, M.A.; Kronstein, M.; Tielens, F. Ionic nanoparticle networks: Development and perspectives in the landscape of ionic liquid based materials. *Chem. Commun.* **2014**, *50*, 10929–10936. [CrossRef] [PubMed]
17. Neouze, M.A. Nanoparticle assemblies: Main synthesis pathways and brief overview on some important applications. *J. Mater. Sci.* **2013**, *48*, 7321–7349. [CrossRef]
18. Herrmann, A.K.; Formanek, P.; Borchardt, L.; Klose, M.; Giebeler, L.; Eckert, J.; Kaskel, S.; Gaponik, N.; Eychmueller, A. Multimetallic Aerogels by Template-Free Self-Assembly of Au, Ag, Pt, and Pd Nanoparticles. *Chem. Mater.* **2014**, *26*, 1074–1083. [CrossRef]

19. Lesnyak, V.; Voitekhovich, S.V.; Gaponik, P.N.; Gaponik, N.; Eychmueller, A. CdTe Nanocrystals Capped with a Tetrazolyl Analogue of Thioglycolic Acid: Aqueous Synthesis, Characterization, and Metal-Assisted Assembly. *ACS Nano* **2010**, *4*, 4090–4096. [CrossRef] [PubMed]
20. Wolf, A.; Lesnyak, V.; Gaponik, N.; Eychmueller, A. Quantum-Dot-Based (Aero) gels: Control of the Optical Properties. *J. Phys. Chem. Lett.* **2012**, *3*, 2188–2193. [CrossRef] [PubMed]
21. Mizuno, K.; Yamaguchi, K.; Kamata, K. Epoxidation of olefins with hydrogen peroxide catalyzed by polyoxometalates. *Coord. Chem. Rev.* **2005**, *249*, 1944–1956. [CrossRef]
22. Venturello, C.; D'Aloisio, R. Quaternary Ammonium Tetrakis(Diperoxotungsto) Phosphates(3-) As A New Class Of Catalysts For Efficient Alkene Epoxidation With Hydrogen-peroxide. *J. Org. Chem.* **1988**, *53*, 1553–1557. [CrossRef]
23. Song, Y.; Tsunashima, R. Recent advances on polyoxometalate-based molecular and composite materials. *Chem. Soc. Rev.* **2012**, *41*, 7384–7402. [CrossRef] [PubMed]
24. Karimi, Z.; Mahjoub, A.R.; Harati, S.M. Polyoxometalate-based hybrid mesostructured catalysts for green epoxidation of olefins. *Inorg. Chim. Acta* **2011**, *376*, 1–9. [CrossRef]
25. Tan, R.; Liu, C.; Feng, N.D.; Xiao, J.; Zheng, W.G.; Zheng, A.M.; Yin, D.H. Phosphotungstic acid loaded on hydrophilic ionic liquid modified SBA-15 for selective oxidation of alcohols with aqueous $H_2O_2$. *Micropor. Mesopor. Mat.* **2012**, *158*, 77–87. [CrossRef]
26. Kamata, K.; Yonehara, K.; Sumida, Y. Efficient epoxidation of olefins with ⩾99% selectivity and use of hydrogen peroxide. *Science* **2003**, *300*, 964–966. [CrossRef] [PubMed]
27. Litschauer, M.; Neouze, M.A. Nanoparticles connected through an ionic liquid-like network. *J. Mater. Chem.* **2008**, *18*, 640–646. [CrossRef]